Eco-friendly Solvent Engineered $CsPbI_{2.77}Br_{0.23}$ Ink for Large-Area and Scalable High Performance Perovskite Solar Cells

Seid Yimer Abate[a], Yifang Qi[a], Qiqi Zhang[a], Surabhi Jha[b], Haixin Zhang[c,d], Guorong Ma[b], Xiaodan Gu[b], Kun Wang[c,d], Derek Patton[b], Qilin Dai[a]*

[a] *Department of Chemistry, Physics, and Atmospheric Sciences, Jackson State University, Jackson, MS, 39217, United States*

[b] *School of Polymer Science and Engineering, Center for Optoelectronic Materials and Devices, The University of Southern Mississippi, Hattiesburg, MS, 39406, United States.*

[c] *Department of Physics, University of Miami, Goral Gables, FL 33124, United States*

[d] *Department of Physics and Astronomy, Mississippi State University, Mississippi State, MS 39762, United States.*

Abstract

The performance of large-area perovskite solar cells has been assessed for typical compositions, such as methylammonium lead iodide ($MAPbI_3$), using a blade coater, slot-die coater, solution shearing, ink-jet printing, and thermal evaporation. However, the fabrication of large-area all-inorganic perovskite films is not well developed. This study developed, for the first time, an eco-friendly solvent engineered all-inorganic perovskite ink of dimethyl sulfoxide as a main solvent with the addition of acetonitrile, 2-methoxyethanol, or a mixture of acetonitrile and 2-methoxyethanol to fabricate large-area $CsPbI_{2.77}Br_{0.23}$ films with slot-die coater at low temperatures (40–50 °C). We thoroughly examined the perovskite phase, morphology, defect

density, and optoelectrical properties of new inks prepared with different solvent ratios and correlated them with their respective colloidal size distribution and solar cell performance. The optimized slot-die-coated $CsPbI_{2.77}Br_{0.23}$ perovskite film, which was prepared from the eco-friendly binary solvents dimethyl sulfoxide:acetonitrile (0.8:0.2 v/v), demonstrated an impressive power conversion efficiency of 19.05%. Moreover, the device maintained *ca.* 91% of its original power conversion efficiency after one month at 20% relative humidity in the dark. We believe that this study will accelerate the reliable manufacturing of perovskite devices.

Keywords: solvent engineering, slot-die coating, all-inorganic perovskite, eco-friendly solvent, binary and ternary solvent

Introduction

All-inorganic perovskites have attracted significant attention for use in tandem solar cells because of their remarkable thermal stability and ideal band gap (> 1.70 eV). The power conversion efficiency (PCE) of organic−inorganic hybrid perovskite solar cells (PSCs) surpasses 26%[1-5] but their poor thermal stability originating from the volatile components such as methylammonium (MA) impedes their practical applications.[6] Therefore, it is necessary to replace the organic cations with inorganic cations such as cesium (Cs^+) to enhance the intrinsic stability of the cells.[6] Efforts to improve the PCE of all-inorganic PSCs, such as defect engineering, have achieved improvements of 20% with promising stability.[7-11] However, these reports had limitations. First, the perovskites were prepared using toxic dimethylformamide (DMF) as the main solvent. Second, the devices were prepared using a simple spin-coating method. These limitations hinder the commercialization of PSCs. Therefore, it is necessary to develop an eco-friendly all-inorganic perovskite ink that can be coated over large areas at low temperatures for the scale-up of such cells

to commercial-size devices with high compatibility for industrial-scale sheet-to-sheet or roll-to-roll processes.

Solvent choice plays a crucial role in perovskite film properties. The solvent Gutmann donor number (D_N) determines the solubility of perovskite precursors, with solvents with a D_N above 18 kcal/mol being able to dissolve lead halides.[12-14] Acetonitrile (ACN), 2-methoxyethanol (2-ME), dimethyl sulfoxide (DMSO), and DMF have a D_N of 14.1, 19.8, 29.8, and 30.9 kcal/mol, respectively.[14,15] Consequently, ACN cannot coordinate with Pb^{2+} nor dissolve halide perovskites, even with the addition of organic cations. 2-ME cannot dissolve PbI_2 but forms a clear perovskite solution with the addition of methylammonium iodide (MAI).[14] DMF and DMSO can dissolve halide perovskites effectively by coordinating with Pb^{2+}; however, DMF is highly toxic. Most highly efficient perovskite devices use DMF as the main solvent and DMSO as an additive in precursor preparation.[3] Besides DMF toxicity, DMF and DMSO have high boiling points and exhibit a highly coordinated nature with perovskite, which requires anti-solvent dripping at the specific very narrow spin-coating window to systematically wash out the coordinating solvents for effective crystallization, which is a significant barrier to scaling up such processes for commercialization. Recently, several solo, binary, and ternary solvents have been introduced without DMF to prepare various compositions of green perovskite inks.[13, 15-21] Sun et. al. employed a mixture of methylammonium acetate and ACN to fabricate high-performance $MAPbI_xBr_{3-x}$ devices, in which the ACN minimized the coordination of the solvent and perovskite solutes that led to the formation of large micelles.[22] Cassella et. al. demonstrated up to 18.0% efficiency for the $MAPbI_3$ PSCs from a binary solvent of 2-ME and tetrahydrofuran. Their process fabricated highly crystalline perovskite layers at room temperature with a gas quencher to remove the solvents without any post-processing steps.[23] In general, solvent parameters such as D_N, vapor

pressure, and boiling point are the key parameters for controlling perovskite crystallization and growth processes via supersaturation.[13] ACN and 2-ME have high vapor pressure values of 9.71 and 0.823 kPa at 20 °C and boiling point values of 82 and 124 °C, respectively. The perovskite solution prepared by the addition of these solvents formed small perovskite crystals associated with the formation of a high density of nuclei via fast evaporation.[12, 24] The perovskite solution based on highly volatile ACN formed a black perovskite layer without any post-treatment at room temperature due to fast nucleation and crystal growth.[16, 24-26] Recently, efficient large-area $MAPbI_3$-based PSCs were fabricated by N_2-knife assisted blade coater by mixing non-coordinating and volatile solvents with coordinating and non-volatile solvents.[14]

The perovskite precursor is generally considered a colloid solution and the colloid nature determines the perovskite film quality and optoelectrical properties.[27-30] This study aimed to develop a $CsPbI_{2.77}Br_{0.23}$ perovskite ink using eco-friendly solvent mixtures of DMSO as the main green solvent and ACN, 2-ME, or ACN/2-ME as additive/secondary solvents. We prepared 21 $CsPbI_{2.77}Br_{0.23}$ perovskite inks by designing various binary and ternary ratios of the coordinating DMSO solvent to the highly vaporized solvents ACN, 2-ME, or ACN/2-ME and studied the precursor colloidal sizes, film morphologies and structures, and device performance. The influence of the colloidal properties of the precursor ink on the performance of devices prepared by a slot-die coater at low temperatures (40–50 °C) was demonstrated. PSCs based on DMSO alone delivered a maximum PCE of 17.80% with a large variance. Intriguingly, the binary eco-friendly solvent-engineered $CsPbI_{2.77}Br_{0.23}$ perovskite ink with DMSO to ACN (DA) ratio of 0.8:0.2 demonstrated an impressive PCE of 19.05% with a short-circuit current (*Jsc*) of 20.91 $mAcm^{-2}$, an open-circuit voltage (V_{oc}) of 1.131V and a fill factor (FF) of 80.57% and high reproducibility.

Furthermore, DA (0.8:0.2) perovskite ink-based devices retained more than 91% of their original PCE after being stored in air for one month at 20% relative humidity (RH) in the dark.

Results and Discussion

A total of 21 $CsPbI_{2.77}Br_{0.23}$ perovskite inks were prepared systematically. Scheme 1 illustrates the preparation of the slot-die-compatible $CsPbI_{2.77}Br_{0.23}$ ink using DMSO, 2-ME, and ACN following a binary and/or ternary solvent mixture approach. The DMSO-based perovskite ink alone was used as the control. ACN or 2-ME alone cannot dissolve $CsPbI_{2.77}Br_{0.23}$ solutes. Intriguingly, by mixing non-coordinating and high-vapor-pressure ACN and 2-ME with DMSO, we slot-die-coated all-inorganic perovskite films at low temperatures over a large area without an additional N_2 knife. We found that a maximum of 50% ACN, 50% 2-ME, or 50% mixture of ACN/2- ME (v/v) could substitute DMSO (v/v) to obtain a clear perovskite ink. Increasing the ratio of volatile solvents above 50% (v/v) led to the formation of a cloudy perovskite ink owing to incomplete dissolution. To find the best solvent ratio for the slot-die coated all-inorganic $CsPbI_{2.77}Br_{0.23}$ films, we optimized the ratio of DMSO to non-coordinating and high-vapor-pressure 2-ME and/or ACN. The precursor colloidal distribution, film morphologies and structures, and device characteristics of the 21 perovskite inks were studied in detail.

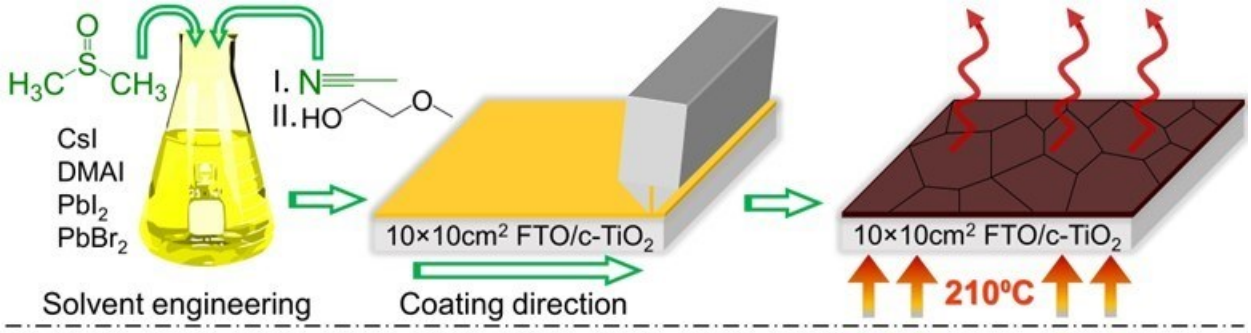

Scheme 1. Schematic illustration of the development of all-inorganic eco-friendly perovskite inks by solvent and colloidal engineering for scalable PSCs. The inks were slot-die coated at 40–50 °C over a large area and annealed at 210 °C for 5 min.

We studied the influence of various mixtures of these solvents on colloidal particle distribution in the perovskite solution, perovskite film morphologies and structures, and device performance. We first investigated the particle size distribution of various solvent-engineered all-inorganic $CsPbI_{2.77}Br_{0.23}$ perovskite precursors using dynamic light scattering (DLS). The individual intensity-weighted DLS size distributions were measured for ten cycles for each fresh precursor solution to maintain consistency across all precursors and the results are summarized in Figure 1a-d. The 21 perovskite precursors were categorized into four groups. The first group (Figure 1a) shows a perovskite precursor prepared from a mixture of DMSO and ACN in short DA at various v/v ratios. The perovskite precursor prepared from DMSO only [DA (1:0)] was characterized by a high size distribution intensity ratio of large particles (> 1000 nm) and low size distribution intensity ratio of small particles (1–5 nm) colloids. However, when ACN was introduced into DMSO [DA (x:y)], the size and size distribution intensity ratio of the large particles decreased. Intriguingly, the binary DA solvent precursors exhibit a high intensity ratio of small particles (1–5 nm). Large aggregate colloidal particles split and formed small colloidal particles with the addition of ACN solvent, which was also observed by Kim et al. upon the addition of I_3^- to $MAPbI_3$ perovskite.[30]

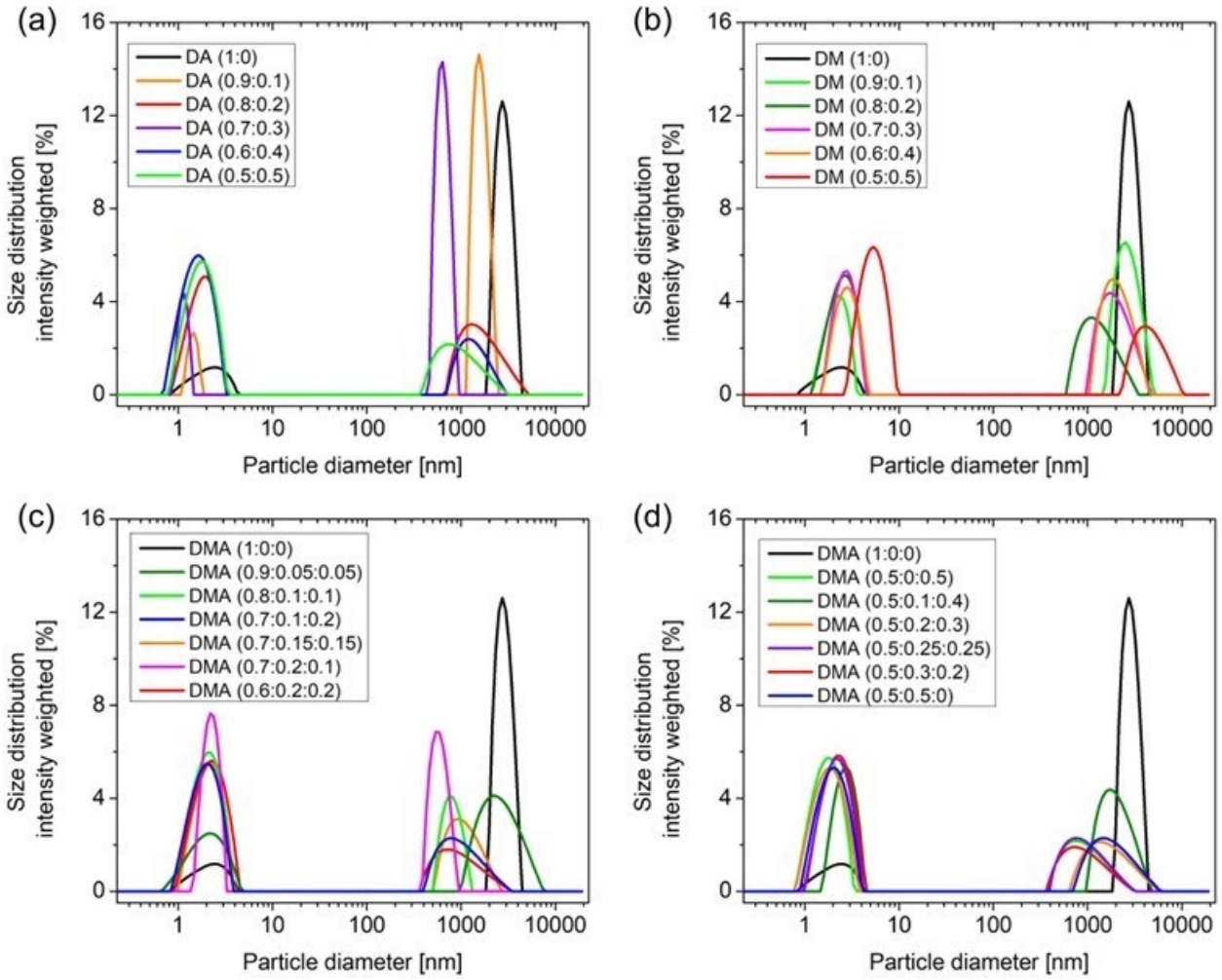

Figure 1. Particle size distributions of various perovskite precursor inks measured by DLS. (a) DA series, (b) DM series, (c) DMA series with varied D, M, and A ratios, and (d) DMA series with maximum MA ratio to D.

We then studied the colloidal size distributions of the perovskite inks prepared from the binary solvents DMSO and 2-ME in a short DM (Figure 1b). A similar trend was observed in the DA system. The size distribution intensity of the smaller particles increased as the amount of 2-ME (0–0.4) increased. However, for DM (0.5:0.5), we observed the highest intensity of small particles. The large particle diameters of the ink prepared with DM (0.5:0.5) increased even above that of the DMSO-only sample, suggesting that both small and large colloids formed in the system.

Further, we investigated the colloidal size distributions of the ternary solvent perovskite precursor solution by mixing DMSO, 2-methoxyethanol, and ACN (hereafter referred to as DMA) in various ratios (Figure 1c-d). Figure 1c shows the particle information of the perovskite solutions with a high volume of DMSO in DMA. However, as shown in Figure 1d, we added maximum amounts of ACN and 2-ME to the main DMSO solvent. The maximum ratio of additive solvents was 50% v/v for both the binary and ternary perovskite precursors. The perovskite solutes could not be dissolved if the additive solvent was over 50% (v/v). In both ternary systems (Figure 1c-d), the intensity of the small colloidal size distribution significantly increased compared to that of the DMSO-only perovskite precursor. The colloidal size distribution and intensity may influence the morphological and optoelectronic properties of the perovskite films. In perovskite film processing, small colloidal sizes provide excellent nucleation sites, which can benefit the formation of compact perovskite layers on slot-die coatings. When the colloid size is large, there is a high possibility of aggregation and the perovskite layer generated from such nucleation sites may have a random morphology associated with many pinholes. In general, the perovskite film quality obtained from the slot-die coating process is influenced by various parameters, including the precursor properties, coating gap, coating speed, coating flow rate, and coating temperature.

We fabricated $CsPbI_{2.77}Br_{0.23}$ perovskite layers using a slot-die coater with various precursors and studied the top-view morphology of the layer using SEM. Figure 2a shows a top-view SEM image of the perovskite layer, where DMSO was the sole solvent used to prepare the precursor and a rough morphology with pinholes was formed. Subsequently, we scanned the top-view perovskite layer prepared from the binary solvents DMSO and ACN mixed in various ratios (Figure 2b-f). When the amount of ACN in the precursor increased, the perovskite grain size increased from 282 to 452 nm (Figure S1 shows the perovskite grain size distributions obtained from the SEM images).

As we employed the same coating parameters for all the precursors, the solvent component influenced the perovskite film morphologies, demonstrating that the film morphologies were related to the initial colloidal size distributions.

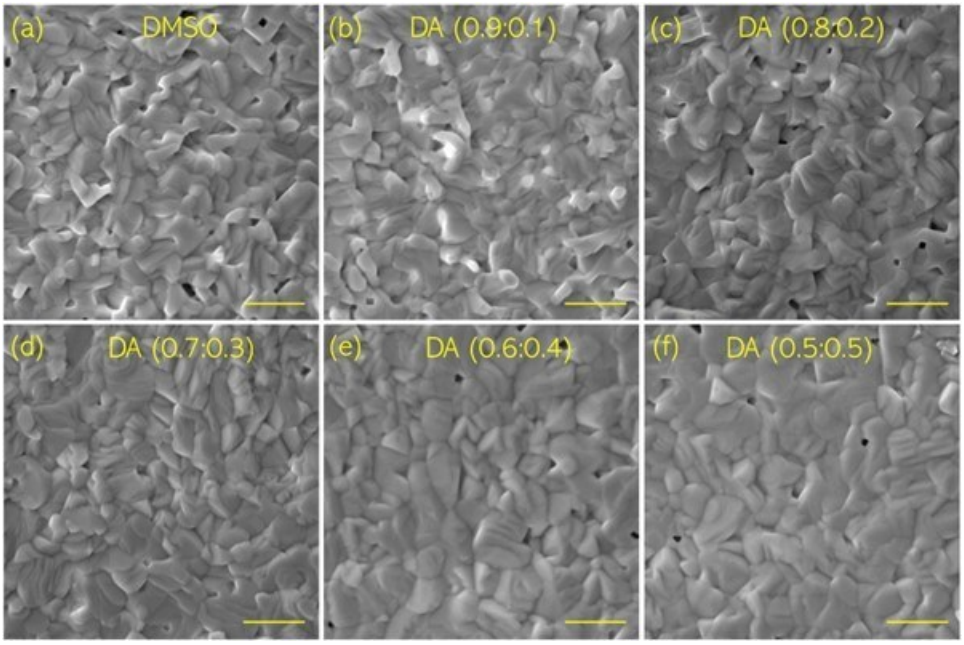

Figure 2. Top-view SEM images of $CsPbI_{2.77}Br_{0.23}$ films prepared from the binary solvent system by mixing DMSO and ACN in various ratios. (a) DMSO only, (b) DA (0.9:0.1), (c) DA (0.8:0.2), (d) DA (0.7:0.3), (e) DA (0.6:0.4), and (f) DA (0.5:0.5).

We studied the top-view morphologies of the perovskite films prepared with various ratios of DMSO to 2-ME (Figure 3a-f). Figure 3a a shows the control perovskite prepared using DMSO solvent. When 2-ME was mixed with small amounts of DMSO, such as DM (0.8:0.2) and (0.7:0.3), compact perovskite layers were formed. A further increase in 2-ME resulted in rough morphologies, particularly for the perovskite layer fabricated using DM (0.5:0.5). Similar to the morphological trend in DA, when the amount of 2-ME increased, the number of perovskite grains increased. Figure S2 shows the size distributions of films prepared using the DM system. However, DM

(0.5:0.5) produced a non-uniform morphology. The DLS of DM (0.5:0.5) showed colloids larger than those formed by DMSO alone. This demonstrates that overly large colloids can result in rough surfaces with substantial numbers of pinholes. Our DLS characterization showed that increased amounts of added ACN or 2-ME in the precursor solution led to a decreased proportion of large colloidal-sized particles, which were responsible for forming the non-uniform perovskite layer, except for DM (0.5:0.5). SEM characterization revealed that the perovskite films prepared using precursors with added ACN or 2-ME produced a uniform morphology compared to the control perovskite films prepared from non-volatile coordinating DMSO only. However, the number of pinholes followed a trend where initially the number of pinholes decreased with the addition of ACN and/or 2-ME and then increased (Figure 2, Figure 3). The modulation of these surface morphologies is related to the variation in the vapor pressure of the different solvents (DA, DM, and DMA). The nucleation and crystal growth of these precursors followed different timescales depending on their ratios, which defined their perovskite surface uniformity and compactness. Perovskite films prepared from the commonly used non-volatile coordinating solvents required a long time to reach supersaturation due to their strong coordination and slow evaporation caused by their high boiling point and low vapor pressure.[12] As a result, discontinuous perovskite layers with pinholes or islands formed.[12] Our control DMSO-prepared perovskite layers also exhibited several pinholes. In contrast, perovskite films prepared from a combination of non-coordinating, low boiling point, and high vapor pressure ACN and/or 2-ME, and a coordinating DMSO [DA, DM, DMA] exhibited faster supersaturation and nucleation rates, resulting in a homogeneous morphology with reduced pinholes. However, when ACN and 2-ME were added to DMSO in different proportions, the boiling points and vapor pressures of the mixed solvents varied significantly and the crystallization kinetics changed accordingly. Note that our inorganic

perovskite could not be dissolved in ACN, 2-ME, or ACN/2-ME mixtures and we employed the partial substitution of DMSO with volatile components to tune the perovskite growth kinetics, perovskite morphology, and optoelectrical properties. Initially, with the addition of small ratios of volatile solvents to DMSO, the number of pinholes was significantly reduced owing to the balanced fast evaporation and crystallization during the formation of the films and the devices produced an improved PCE. However, when the ratio of ACN and/or 2-ME in DMSO was further increased, the solubility of the perovskite decreased. The small colloidal particle size distribution decreased and the large colloidal particle size distribution increased, which negatively influenced the perovskite morphology, leading to increased pinhole formation. Overall, the solvent ratio significantly influenced the film's growth and quality.

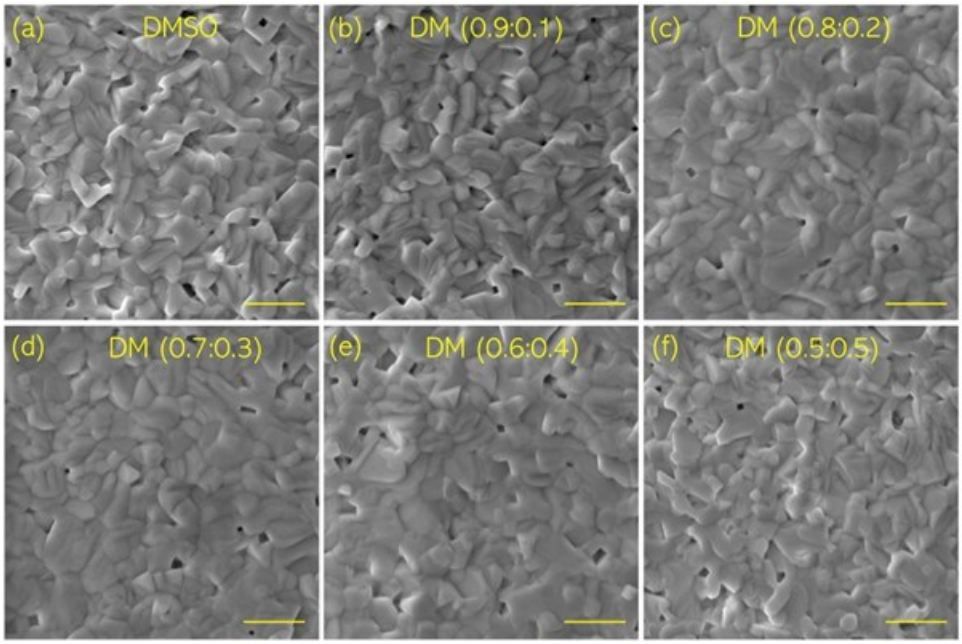

Figure 3. Top view SEM images of $CsPbI_{2.77}Br_{0.23}$ films prepared from DM system: (a) DMSO only, (b) DM (0.9:0.1), (c) DM (0.8:0.2), (d) DM (0.7:0.3), (e) DM (0.6:0.4), and (f) DM (0.5:0.5).

We studied the top-view morphologies of slot-die-coated $CsPbI_{2.77}Br_{0.23}$ perovskite layers prepared using ternary solvents (DMA) (Figure 4a-l). Small amounts of ACN, 2-ME, and 2-ME/ACN in the perovskite precursor did not benefit the coating process, and the morphologies were similar to those of the perovskite films prepared using DMSO alone. Consequently, the perovskite films prepared with DA (0.9:0.1), DM (0.9:0.1), and DMA (0.9:0.05:0.05) exhibited rough surfaces. When non-coordinating (2-ME/ACN) solvents were employed together with DMSO in the ternary solvent approach to prepare the perovskite solution, the ratio of 2-ME to ACN significantly affected the film morphology. Figure 4a-f shows the morphologies of the films based on the ternary solvents with different ratios of 2-ME and ACN. The films prepared with DMA (0.8:0.1:0.1), DMA (0.7:0.1:0.2), DMA (0.7:0.15:0.15), and DMA (0.7:0.2:0.1) exhibited uniform morphologies; however, the film prepared with DMA (0.6:0.2:0.2) was rougher and exhibited more pinholes. Finally, we studied the top-view morphologies of the perovskite layers when the DMSO amount was half the ratio and 2-ME/ACN was the other half ratio to prepare the perovskite solution. Figure S3 shows the grain-size distribution of the films. When the amount of ACN decreased and 2-ME increased, the perovskite particle sizes decreased from 393 to 324 nm (Figure S3 c-e) and from 436 to 349 nm (Figure S3 g-k), respectively, and the perovskite morphologies became rougher (Figure 4g-l). The morphological studies demonstrated that tuning the precursor solvent/ratio from DMSO alone to binary and ternary solvents could lead to effective control of perovskite morphologies. The morphology trend was similar to the colloidal size distribution trend, and a more detailed study is required.

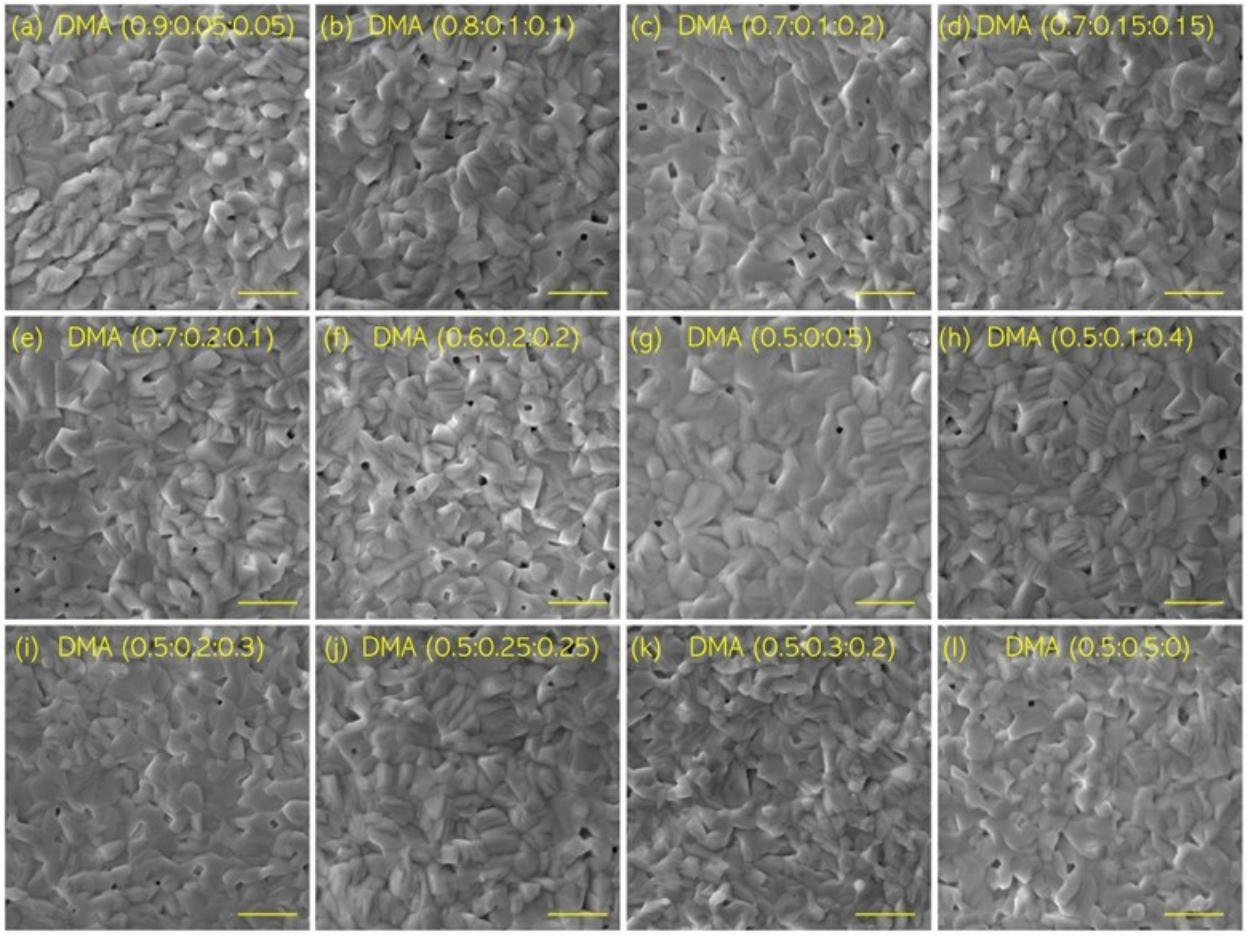

Figure 4. Top-view SEM images of $CsPbI_{2.77}Br_{0.23}$ films prepared with the ternary solvent system by mixing DMSO, 2-ME, and ACN in various ratios: (a) DMA (0.9:0.05:0.05), (b) DMA (0.8:0.1:0.1), (c) DMA (0.7:0.1:0.2), (d) DMA (0.7:0.15:0.15), (e) DMA (0.7:0.2:0.1), and (f) DMA (0.6:0.2:0.2). (g) DMA (0.5:0:0.5), (h) DMA (0.5:0.1:0.4), (i) DMA (0.5:0.2:0.3), (j) DMA (0.5:0.25:0.25), (k) DMA (0.5:0.3:0.2), and (l) DMA (0.5:0.5:0).

We fabricated planar PSCs with a structure of FTO/c-TiO_2/ $CsPbI_{2.77}Br_{0.23}$ /Spiro-OMeTAD/Au based on inorganic perovskite films obtained using our inks. Figure 5a-d shows the J-V curves of PSCs based on various binary DA solvents. The control device based on a sole DMSO solvent exhibited a maximum PCE of 17.80% with a J_{sc} of 20.71 $mAcm^{-2}$, V_{oc} of 1.109 V, and FF of 77.49%. The low device performance was attributed to the poor film morphology, which resulted

in leakage current and poor interface contact that ultimately deteriorated the device PCE.[22] When ACN was added to the DMSO, the efficiency of the device improved remarkably. The devices based on DA (0.8:0.2) showed the best PCE of 19.05%, with a J_{sc} of 20.91 mAcm^{-2}, V_{oc} of 1.131V, FF of 80.57%, and high process reproducibility. The performance of various binary DA solvent-based devices is summarized in Table S1.

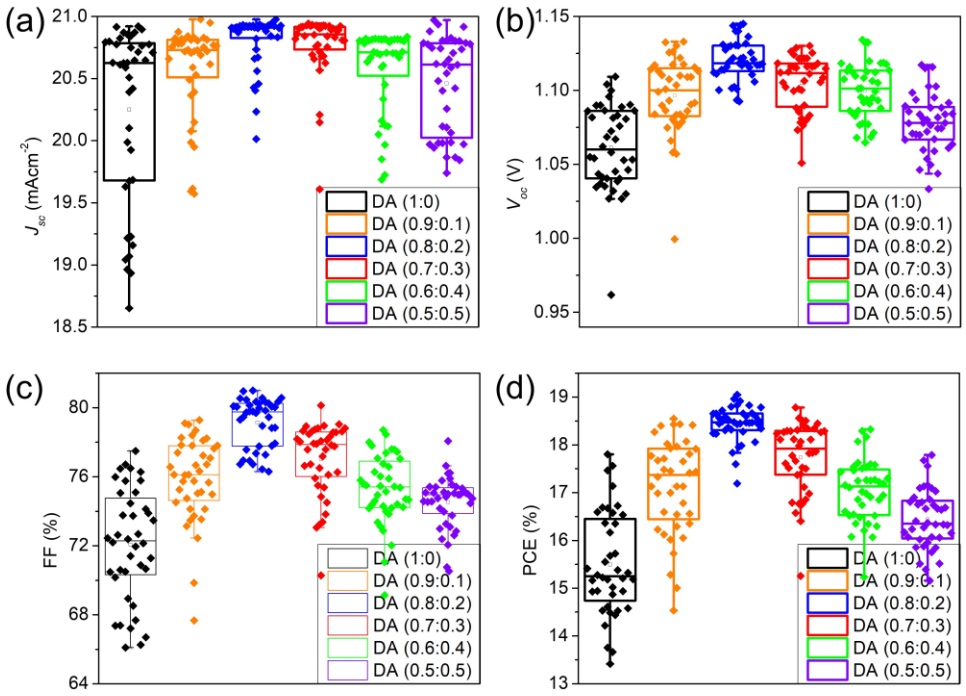

Figure 5. Photovoltaic parameters of the devices based on DA solvents.

We fabricated DM-precursor-based PSCs, and the results are summarized in Figure 6. The DM (0.8:0.2)-and DM (0.7:03)-based devices exhibited excellent PCE of 18.25% and 18.51%, respectively. The DM (0.7:0.3)-based device exhibited a J_{sc} of 20.84 mAcm^{-2}, V_{oc} of 1.124V, and FF of 79.03%. However, when the amount of 2-ME increased, the PCE of the DM-based device decreased. The PCE of the device based on DM (0.5:0.5) was 17.46%. A summary of the PCE based on the DM system is presented in Supplementary Table S2.

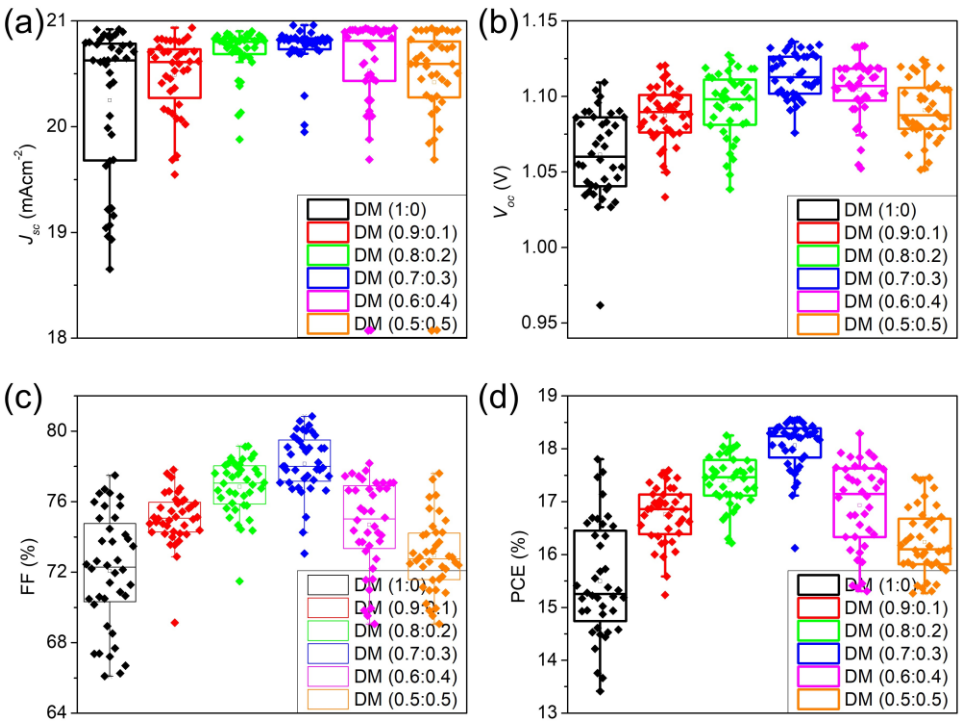

Figure 6. Photovoltaic parameters of the devices based on DM solvents.

Similarly, we fabricated PSCs based on ternary solvent mixtures of DMSO, 2-ME, and ACN, and the device characterizations are summarized in Figure S4–S5 and Tables S3–S4. The DMA (0.7:0.15:0.15)-based device exhibited a J_{sc} of 20.93 mAcm^{-2}, V_{oc} of 1.111V, FF of 79.00%, and maximum PCE of 18.37%. Stretching the amount of 2-ME and ACN to 50% to minimize the amount of the main DMSO solvent resulted in a PCE similar to that of the DMSO-based device; however, the reproducibility was significantly improved. J-V studies indicated that perovskite films fabricated using binary solvents (DA and DM) produced better device performances than those fabricated using the ternary solvent system. We studied the reproducibility of the devices based on 21 solvents, and the histogram data are shown in Figure S6a-d, where devices with DA (0.8:0.2) and DM (0.7:0.3) demonstrated impressive PCEs and high reproducibility.

We studied the compositional, optoelectrical, and structural properties of perovskite films prepared using DMSO (D), DA (0.8:0.2), and DM (0.7:0.3) solvents. Figure 7a shows the FTIR spectra of the three films, which exhibit similar functional groups without peak shifting because the additive solvents 2-ME and ACN were completely removed from the films. The UV-Vis absorption spectra of the perovskite films prepared from D, DA (0.8:0.2), and DM (0.7:0.3) exhibited overlapping features with an absorption onset at 729 nm (Figure 7b). Figure 7c shows the X-ray diffraction (XRD) data of the perovskite films prepared from D, DA (0.8:0.2), and DM (0.7:0.3), with all films exhibiting highly crystallized $CsPbI_{2.77}Br_{0.23}$ perovskites. Furthermore, we applied 2D-GIWAXS to study the detailed structure of the perovskites prepared with D, DA (0.8:0.2), and DM (0.7:0.3), and a pure perovskite phase without remnants was observed (Figure 7d-g). Next, we investigated the charge recombination properties of slot-die-coated $CsPbI_{2.77}Br_{0.23}$ perovskite films prepared from D, DA (0.8:0.2), and DM (0.7:0.3). Figure 7h shows the steady-state PL spectra of the different perovskite films on glass, where all films exhibited an emission peak at 720 nm. The three films exhibit similar thicknesses (Figure S7). Intriguingly, the perovskite films prepared from DA (0.8:0.2) demonstrated a significant PL enhancement of 91% compared to the DMSO solvent-prepared layer. Additionally, the DM (0.7:0.3)-based film exhibited a 59% PL enhancement. These PL enhancements for the DA (0.8:0.2)-and DM (0.7:0.3)-based films suggest that charge recombination was suppressed in the binary solvent-prepared perovskite films compared to the DMSO-prepared film. We employed time-resolved PL (TRPL) was used to calculate the charge carrier lifetimes of the perovskite films prepared from D, DA (0.8:0.2), and DM (0.7:0.3) (Figure 7i). The average charge carrier lifetimes τ_{avg} were calculated using equations (1–2).[26] DA (0.8:0.2)-processed perovskite layer exhibited an extremely long average charge carrier lifetime (228.30 ns) compared to the DMSO-prepared perovskite film (120.78 ns). DM

(0.7:0.3) exhibited an average charge carrier lifetime of 221.32 ns. The charge carrier lifetimes are summarized in Table S5.

$$Y = A_1 \exp\left(\frac{-t}{\tau_1}\right) + A_2 \exp\left(\frac{-t}{\tau_2}\right) \quad (1)$$

$$\tau_{avg} = \frac{A_1 {\tau_1}^2 + A_2 {\tau_2}^2}{A_1 \tau_1 + A_2 \tau_2} \quad (2)$$

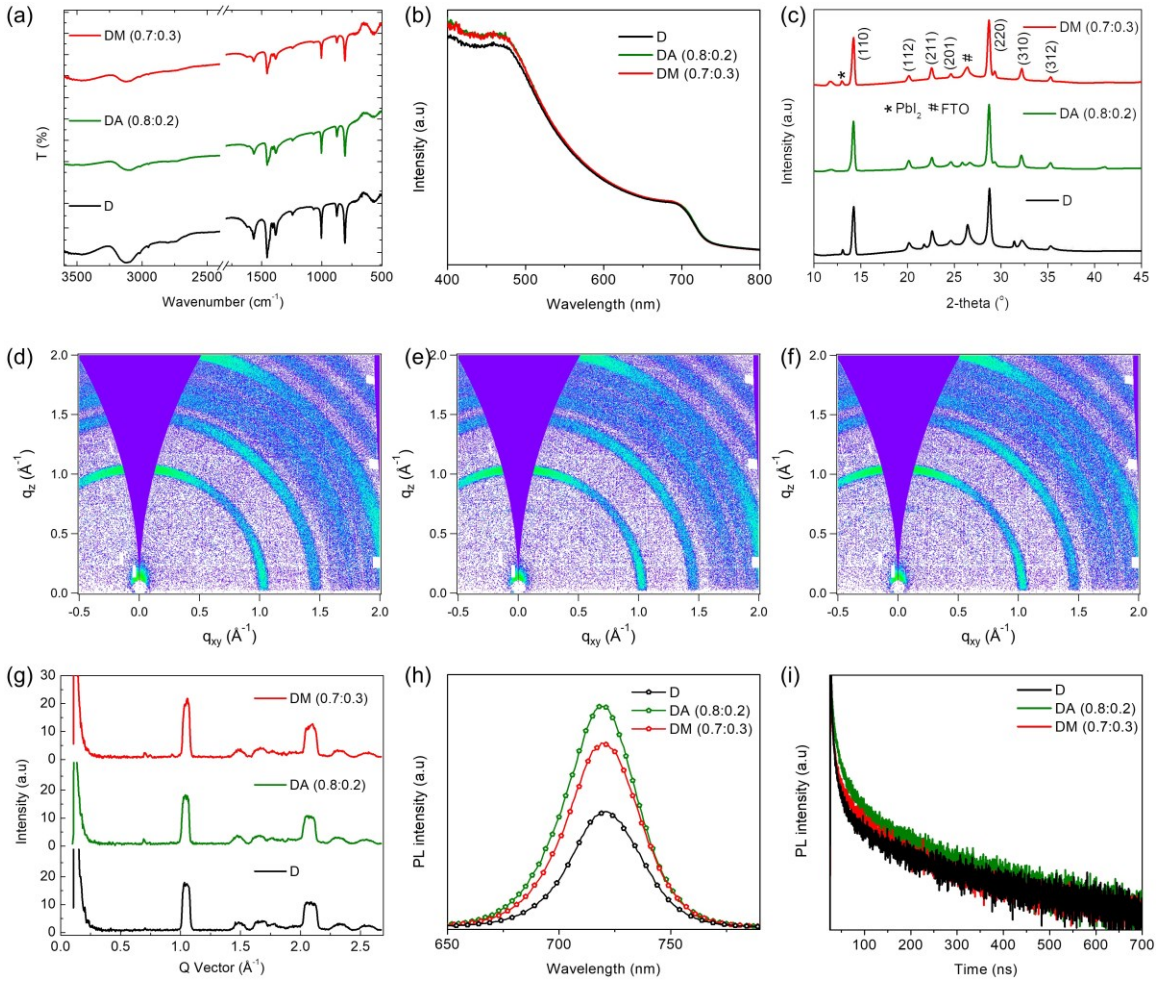

Figure 7. (a) FTIR spectra, (b) UV-vis absorption spectra, and (c) XRD data of $CsPbI_{2.77}Br_{0.23}$ prepared from D, DA (0.8:0.2), and DM (0.7:0.3). 2D-GIWAXS of $CsPbI_{2.77}Br_{0.23}$ films prepared

using (d) D, (e) DA (0.8:0.2), and (f) DM (0.7:0.3). (g) Azimuthally integrated profile, (h) PL, and (i) TRPL of $CsPbI_{2.77}Br_{0.23}$ films prepared from D, DA (0.8:0.2), and DM (0.7:0.3) solvents.

The morphology, crystallinity, compactness, and homogeneity of perovskite films are critical for obtaining high-quality films and high-performance devices. Perovskite crystals and/or films with structural and electronic defects exhibit poor device efficiencies. The final perovskite films formed by slot-die coating were composed of polycrystalline perovskite grains, and the perovskite film properties were highly influenced by the choice of solvents. Solvents influence the solubility of the inorganic perovskite components, chemical reactions, colloidal size distribution, and crystallization kinetics, which determine the quality of the perovskite film, density of defects, optoelectrical properties, and overall device performance. For our control sample, we employed high boiling point highly coordinated polar aprotic DMSO to dissolve the perovskite precursor, and it produced non-homogenous, dendritic films with pinholes/grain boundaries (Figure 2a) due to a lower degree of supersaturation (slower nucleation rate and faster crystal growth rate), which led to the formation of a large density of perovskite defects.[12] We engineered the solvent ratios in the DA, DM, and DMA systems by mixing the DMSO with various amounts of volatile and non-coordinating solvents such as ACN and/or 2-ME. We created a high degree of supersaturation (faster nucleation rate and slower crystal growth rate) at the optimized ratios, which resulted in highly uniform and compact perovskite layers with a reduced density of defects. In general, the choice of solvent for dissolving any perovskite precursor depends on the Gutmann donor number, dielectric constant, and Mayer bond order. The solvents not only determine the solubility of the perovskite but also the crystallization kinetics (nucleation and crystal growth rate). The degree of supersaturation is significantly influenced by the solvent boiling point, coordination with the

perovskite precursor, and solvent vapor pressure. Solvents affect the perovskite crystallization kinetic rates and solubility patterns, which in turn influence the perovskite density of defects.

We performed an XPS survey of the perovskite films prepared from D, DA (0.8:0.2), and DM (0.7:0.3) to investigate their elemental compositions (Figure S8). No peak shift was observed in the three solvent systems, with the final perovskite composition consistent for all samples. XPS measurements were performed to determine the atomic ratios of the perovskite films (Table S6). The Cs:Pb:I ratio was approximately 1:1:3 and the Br:I ratio was 1:28.4. Very little Br was doped into the films, which was consistent with the EQE data. No blue shift was observed, indicating that a very small amount of Br was doped into the films. Figures 8a-f and S9 show the surface roughness and AFM phase images of $CsPbI_{2.77}Br_{0.23}$, respectively. Surface roughness values of 30.4, 32.3, and 34.9 nm were obtained for D, DA (0.8:0.2), and DM (0.7:0.3), respectively. The phase images were consistent with the roughness data. Electron and hole traps influence charge transport and overall device performance. We fabricated electron-only devices with the structure FTO/c-TiO_2/ $CsPbI_{2.77}Br_{0.23}$/PCBM/Au (Figure 8g-i) and hole-only devices with the structure FTO/PEDOT:PSS/$CsPbI_{2.77}Br_{0.23}$/Spiro-OMeTAD/Au based on films prepared with D, DA (0.8:0.2), and DM (0.7:0.3) (Figure 8j-l). The device fabrication procedures and fitting equations were adopted from the literature.[26] The trap density was calculated using equation 3.

$$N_{traps} = \frac{2\varepsilon\varepsilon_0 V_{TFL}}{eL^2} \quad (3)$$

where N_{traps} is the trap density, ε is the relative dielectric constant of $CsPbI_3$,[31] ε_0 is vacuum permittivity, V_{TFL} is trap-filled limit voltage, e is the elementary charge, and L is the thickness of perovskite films. The control device based on $CsPbI_{2.77}Br_{0.23}$ ink prepared with solvent D exhibited an electron trap density of 5.08×10^{15} cm^{-3}. Intriguingly, the electron trap density was significantly

suppressed to 1.18×10^{15} cm^{-3} and 1.84×10^{15} cm^{-3} when $CsPbI_{2.77}Br_{0.23}$ inks were prepared using DA (0.8:0.2) and DM (0.7:0.3), respectively. The trap density of the DA (0.8:0.2) $CsPbI_{2.77}Br_{0.23}$ ink-based device was approximately 76% lower than that of the control device, which could be the main reason for the high PL intensity of the film.

We then fabricated hole-only devices to study the hole trap density of the films prepared with D, DA (0.8:0.2), and DM (0.7:0.3) inks. The control device showed a hole-trap density of 1.27×10^{15} cm^{-3}. DA (0.8:0.2) and DM (0.7:0.3)-based devices exhibited decreased hole-trap density of 0.96×10^{15} cm^{-3} and 0.98×10^{15} cm^{-3}, respectively. The electron and hole trap densities are summarized in Table S7. The reduced defects had a positive influence on the V_{oc} and FF of the cells.[7,32]

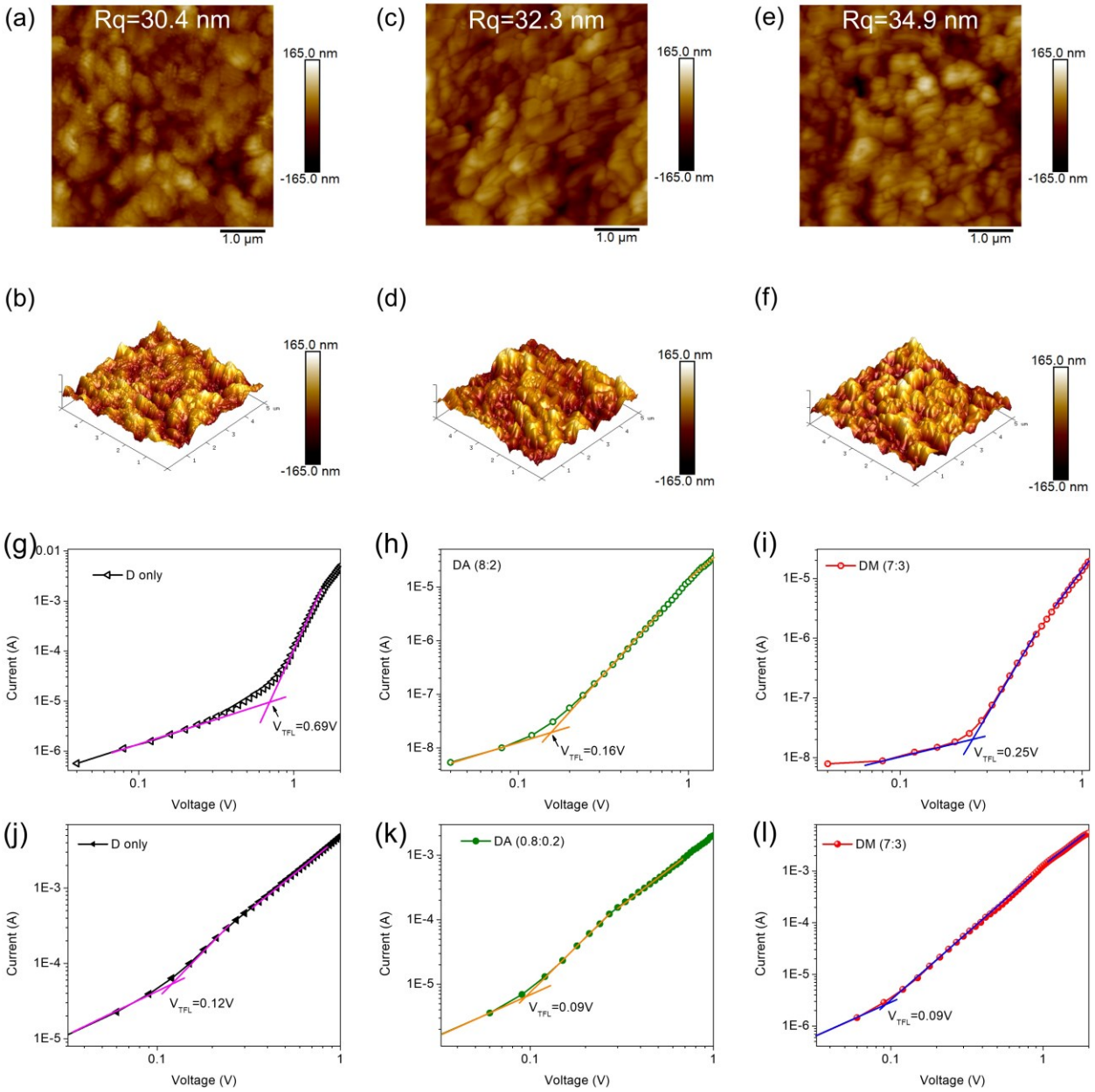

Figure 8. AFM topographic and 3D-images of $CsPbI_{2.77}Br_{0.23}$ films prepared using solvents (a-b) D, (c-d) DA (0.8:0.2), and (e-f) DM (0.7:0.3), respectively. Current-voltage (I-V) curves of electron-only devices based on $CsPbI_{2.77}Br_{0.23}$ films prepared using solvents (g) D, (h) DA (0.8:0.2), and hole-only devices based on (i) DM (0.7:0.3), (j) D, (k) DA (0.8:0.2), and (l) DM (0.7:0.3).

The energy-level alignment of the perovskite layer influenced the charge transfer in the devices. Figure 9a-c shows the $E_{cut\text{-}off}$ and E_{HOMO} of $CsPbI_{2.77}Br_{0.23}$ films prepared using D, DA (0.8:0.2), and DM (0.7:0.3) solvents measured using UPS. The three solvents barely influenced the energy levels of the perovskite layers. Subsequently, we calculated the band gap of perovskite layers by the Tauc plot and found that all three curves overlapped and all $CsPbI_{2.77}Br_{0.23}$ films exhibited a bandgap of 1.70 eV (Figure 9d). The energy-level alignment of the $CsPbI_{2.77}Br_{0.23}$ layer with respect to the other layers in the device is presented in Figure 9e. Kelvin probe force microscopy was employed to measure the contact potential difference (CPD) of the $CsPbI_{2.77}Br_{0.23}$ perovskite films prepared from D, DA (0.8:0.2), and DM (0.7:0.3) (Figure 9f). The control sample exhibited −350 mV relative to the tip. Intriguingly, the perovskite film prepared using the DA (0.8:0.2) solvent exhibited a significant enhancement compared to the control perovskite film (ca. 250 mV to the tip). Moreover, the perovskite prepared by DM (0.7:0.3) exhibited an enhanced CPD compared with that of the control film. The CPD results suggest that a very high potential was formed in the DA (0.8:0.2)-based films, which could be beneficial for charge transport, and V_{oc} enhancement was expected in these devices. The CPD data were consistent with the PL, electron, and hole trap studies, where V_{oc} was highly correlated with the trap density. The film based on DA (0.8:0.2) exhibited the lowest trap density and highest PL intensity compared to the other films, indicating the significant potential of the high Voc of the cells.

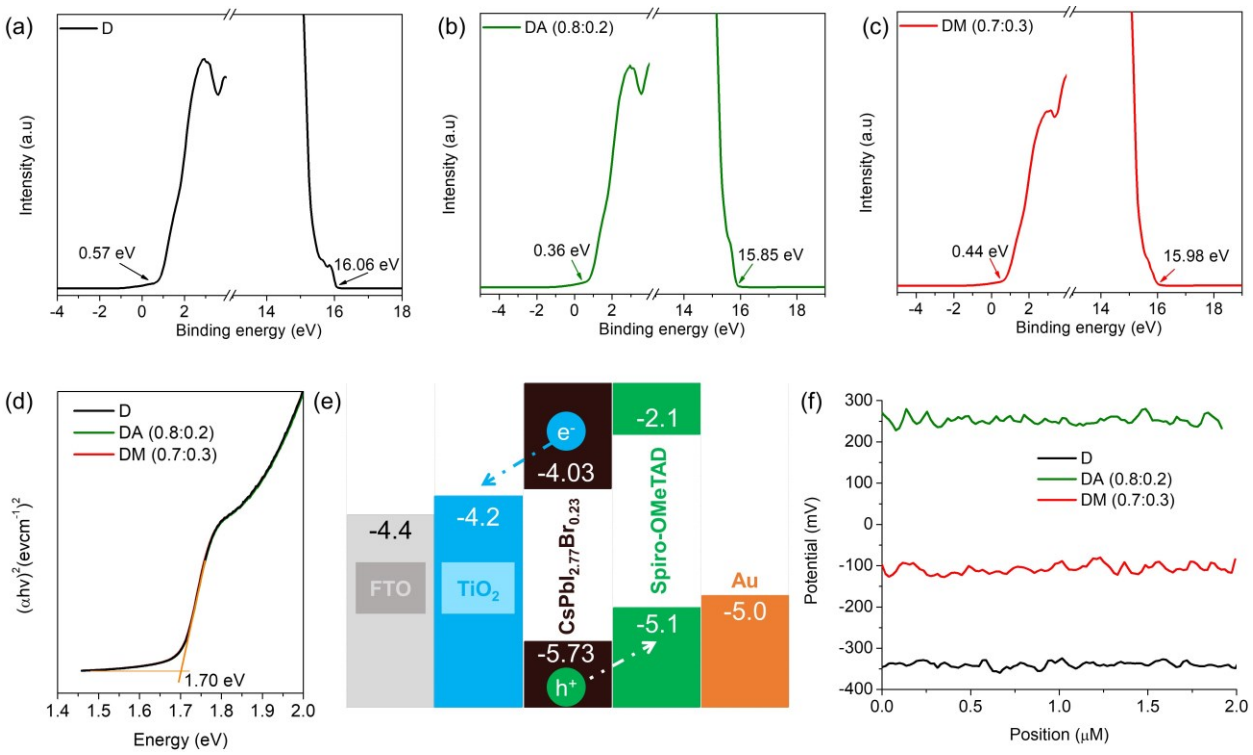

Figure 9. UPS spectra of $CsPbI_{2.77}Br_{0.23}$ films prepared using solvents (a) D, (b) DA (0.8:0.2), and (c) DM (0.7:0.3). (d) Tauc plot of $CsPbI_{2.77}Br_{0.23}$ films prepared using D, DA (0.8:0.2), and DM (0.7:0.3) solvent. (e) energy level alignment diagram of the perovskite layer with respect to other layers in the devices with a structure of FTO/c-TiO_2/$CsPbI_{2.77}Br_{0.23}$/spiro-OMeTAD/Au. (f) Contact potential difference of various $CsPbI_{2.77}Br_{0.23}$ films measured using Kelvin probe force microscopy.

We fabricated PSCs with a structure of FTO/c-TiO_2/$CsPbI_{2.77}Br_{0.23}$/Spiro-OMeTAD/Au, where perovskite inks were prepared using D, DA (0.8:0.2), and DM (0.7:0.3) solvents. The device parameters are summarized in Figure 10a-d, with the device with DA (0.8:0.2) demonstrating the highest performance and a narrow statistical distribution (Figure 10e). Figure 10f-h shows the best performance of the PSCs prepared using the D, DA (0.8:0.2), and DM (0.7:0.3) solvents. The control device demonstrated a maximum PCE of 17.80% under reverse bias and 16.97% under

forward bias, with a hysteresis index (HI) of 4.66%. Interestingly, the device prepared with the DA (0.8:0.2) solvent demonstrated a superior PCE of 19.05% with a reduced HI of 2.67%. Furthermore, the DA (0.8:0.2) solvent-based device exhibited the highest V_{oc} of 1.132 V and FF (80.57 %). This indicates that structural and/or electronic defects in the perovskite films were suppressed using our eco-friendly DMSO/ACN mixed solvent. Our results were achieved using green solvents and slot-die-prepared perovskite layers, which is one step closer to commercializing all-inorganic PSCs. In addition, the device based on DM (0.7:0.3) exhibited a maximum PCE of 18.51% and HI of 2.49%. The stabilized PCE data of the control, DA (0.8:0.2), and DM (0.7:0.3) solvent-prepared devices are presented in Figure 10i. All the devices exhibited stable PCE at their corresponding maximum power point (MPP) for 300 s, which inferred that the all-inorganic PSCs were highly stable. Subsequently, we studied the details of the charge dynamics process by electro-impedance spectroscopy (EIS) in the dark. EIS was used to inspect the series resistance, capacitance, and charge recombination resistance of the devices. Figure 10j shows the EIS plot recorded at a 0.91 V bias and their equivalent circuit is presented in Figure S10. The fitting results are summarized in Table S8. The semi-circle in the high-frequency region was correlated to the charge recombination resistance and geometrical capacitance.[26] The control device with DMSO solvent only showed a series resistance (R_s) of 60.83 Ω, and this parameter was reduced to 39.37 Ω for the device based on DA (0.8:0.2) ink. Intriguingly, the charge recombination resistance (R_{rec}) significantly was improved (> ten-fold) for the DA (0.8:0.2) ink-prepared device compared to the control device (2079 Ω vs 177.40 Ω), which conclusively confirmed that the perovskite defects were successfully repressed in the DA (0.8:0.2)-based device, leading to enhanced photovoltaic parameters in the device. Figure 10k shows the EQE of the devices. The integrated J_{sc} values of the D, DA (0.8:0.2), and DM (0.7:0.3) solvent-based devices were 18.39, 18.85, and 18.63 mA

cm^{-2}, respectively. The discrepancy between the integrated J_{sc} and J_{sc} obtained from the J-V curves was within 20%, suggesting reasonable data.[33]

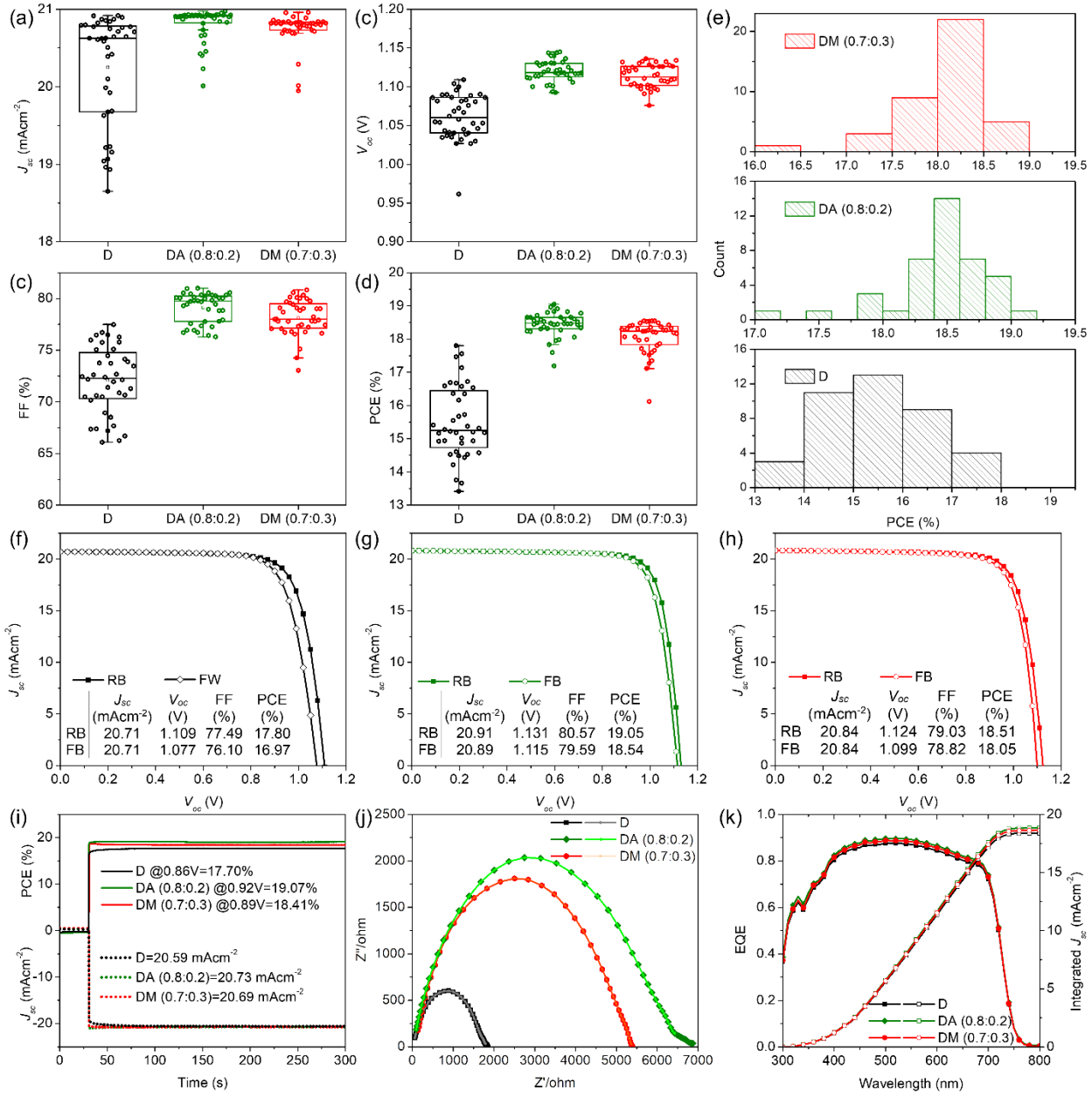

Figure 10. (a-d) Champion photovoltaic parameters of $CsPbI_{2.77}Br_{0.23}$-based devices prepared using D, DA (0.8:0.2), and DM (0.7:0.3) inks. (e) PCE histograms of PSCs using D, DA (0.8:0.2), and DM (0.7:0.3) inks. J-V curves of the champion devices are based on (f) D, (g) DA (0.8:0.2), and (h) DM (0.7:0.3). (i) Stabilized power output of the control device at MPP = 0.86 V, DA

(0.8:0.2)-based device at MPP=0.92 V, and DM (0.7:0.3)-based device at MPP=0.89 V. (j) Nyquist plots and (k) EQE of devices based on D, DA (0.8:0.2), and DM (0.7:0.3).

Finally, we studied the long-term stability of the PSCs prepared from D, DA (0.8:0.2), and DM (0.7:0.3) inks (Figure 11). For reliability testing, we measured the four devices every four days for one month. The devices were stored in air at RH below 20% in the dark. The control device maintained approximately 70% of its original PCE. Intriguingly, the DA (0.8:0.2)- and DM (0.7:0.3)-based devices maintained more than 90% of their initial PCE under the same conditions and durations. Figure S11 shows the operational stability of devices prepared using different solvents. When testing the thermal stability under 85 °C, the devices based on D:A (0.8:0.2) and D:M (0.7:0.3) maintained ~80% of the original PCE, compared to ~55% for the control device (Figure S11 a). When subjected to MPP tracking for 200 h, the devices based on D:A (0.8:0.2) and D:M (0.7:0.3) maintained 90% and 80% of their original PCE, respectively, compared with 50% for the control device (Figure S11 b). The improved device stability was attributed to the high-quality perovskite films with few defects prepared using the engineered solvent method. A solar module with 6 sub-cells and an area of 10 x 10 cm^2 was fabricated based on the solvent of D:A (0.8:0.2) and achieved a PCE of 8.07%, as shown in Figure S12 a. Figure S12b shows the stability of the solar module, showing that 54% of the original PCE was maintained when the module was stored in air in the dark for ~250 h (RH < 20%). The device with an active area of 2.5 x 2 cm^2 obtained a PCE of 16.03%, as shown in Figure S12 c and d. The device maintained approximately 85% of its initial PCE when stored in air in the dark for 250 h (RH < 20%).

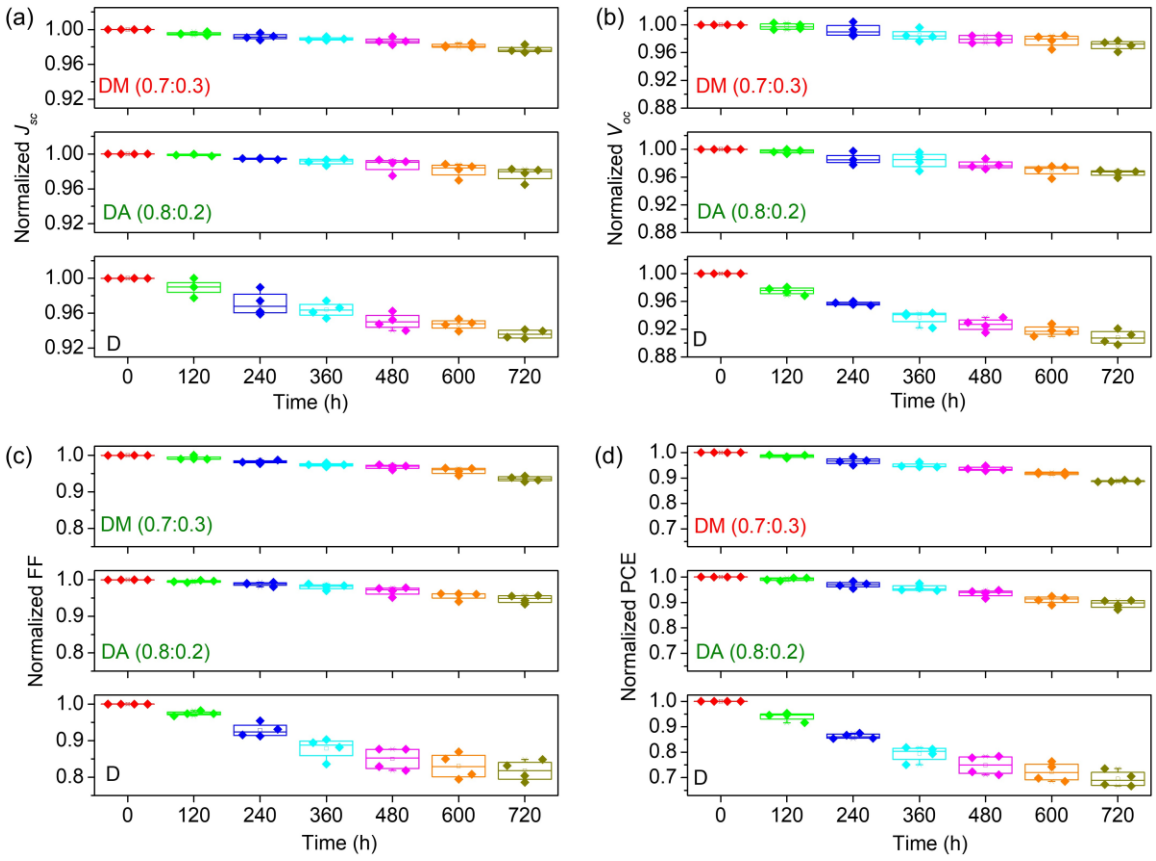

Figure 11. Long-term device stability of $CsPbI_{2.77}Br_{0.23}$-based devices: (a) short-circuit current (J_{sc}), (b) open-circuit voltage (V_{oc}), (c) fill factor (FF), and (d) PCE. The devices were stored in the air at RH below 20% in the dark.

Conclusion

All inorganic perovskite inks for a slot-die coater with a composition of $CsPbI_{2.77}Br_{0.23}$ were developed from eco-friendly binary and ternary mixed solvents for the first time using coordinating DMSO and non-coordinating and highly volatile ACN and 2-ME. DLS investigations showed that the number of small particles (<10 nm) increased when the amount of volatile ACN, 2-ME, and the ACN/2-ME ratio increased. Perovskite films with uniform and compact morphology can be achieved by mixing coordinating solvents and highly volatile non-coordinating solvents, rather than using DMSO alone. We found that optimum ratios of the two solvents are required to achieve

high-quality perovskite layers. With an optimized ratio of DA (0.8:0.2), the PSCs demonstrated excellent optoelectrical and J-V properties, with a superior PCE of 19.05%. The control DMSO-based device exhibited a low average V_{oc} and FF and less reproducibility owing to the nonuniform film formation caused by the strong coordination of DMSO in the slot-die coating. The device prepared using 50% DMSO and 50% volatile solvents displayed a PCE comparable to that of the control solvent and improved reproducibility. Our ecofriendly all-inorganic perovskite inks for slot-die coaters can be employed in roll-to-roll or sheet-to-sheet processes for further optimization. This study opens a new avenue for the development of green and scalable perovskite inks for the commercialization of PSCs.

Experimental Section

Materials. FTO substrates were purchased from Youxuan TECH (China). Cesium iodide (CsI) was acquired from STREM Chemicals, Inc. Dimethylammonium Iodide (DMAI) was purchased from GreatCell Solar Materials. Lead iodide (PbI_2) and lead bromide ($PbBr_2$) were obtained from TCI Chemicals.

Device Fabrication. The FTO patterning and cleaning protocol,[32, 34-37] and c-TiO_2 layer preparation were adopted from our previous literature.[16, 26] 0.8 M $CsPbI_{2.77}Br_{0.23}$ perovskite inks were prepared by mixing 0.208 g CsI, 0.208 g DMAI, 0.306 g PbI_2, and 0.050 g $PbBr_2$ with various compositions of eco-friendly solvents, such as dimethyl sulfoxide (DMSO = D), acetonitrile (ACN=A), and 2-Methoxyethanol (2-ME=M). A total of 21 perovskite precursor solutions were prepared. Subsequently, the perovskite inks were slot-die coated on 10×10 cm^2 c-TiO_2 at a coating speed of 1.5 mm^{-1}, flowrate of 2.28 μLs^{-1}, and coating gap of 75 μm at 40–50 °C and less than 20%

RH. Subsequently, the wet films were annealed at 210 °C for 5 min. To study the photovoltaic parameters, the large area perovskite films were cut to small sizes of 1.5×1.5 $cm^{2,}$ and the spiro-OMeTAD hole-transport layer was coated according to our previous publication.[35] Finally, an Au electrode (80 nm) was prepared following our work.[32]

DLS Sample Preparation. To study the colloidal size distribution of the perovskites, various solvent-engineered perovskite inks (1.5 mL) were prepared. Fresh samples with similar preparation durations and protocols were used to remove the influence of ink aging on the colloidal sizes. Each DLS measurement was recorded over ten cycles.

Film / Device Characterizations. X-ray diffraction (XRD), grazing incidence wide-angle x-ray scattering (2D-GIWAXS), Fourier-transform infrared spectroscopy (FTIR), ultraviolet Photoemission Spectroscopy (UPS), x-ray photoelectron spectroscopy (XPS), ultraviolet-visible (UV−vis) absorption, photoluminescence (PL), Time-resolved photoluminescence (TRPL), Kelvin probe force microscopy (KPFM), contact potential difference (CPD), maximum power point (MPP), electro-impedance spectroscopy (EIS) and scanning electron microscope (SEM) were employed to study the structural, morphological, and optoelectrical properties of the $CsPbI_{2.77}Br_{0.23}$ films following our previous work.[26, 32] Current density–voltage (J−V) and external quantum efficiency (EQE) of the perovskite devices were recorded using the same equipment and conditions as in our previous work.[35] The active area of the devices was 0.1 cm^2.

Statistics: Figures S1–S3 show the mean size obtained by counting the sizes of approximately 100 particles and plotting the size distribution using Origin 2018. The average values in Figures S4–S5, Figures 5–6, and 10–11 were obtained using the software Origin Statistics function.

ASSOCIATED CONTENT

Supporting Information

Extended tables, box charts, histograms, AFM images, and XPS spectra.

Notes

The authors declare no competing financial interest.

Acknowledgments

Q. D. thanks the DOE SIPS program for its financial support (award number EE0010242). This work was also partially supported by the National Science Foundation (DMR- 2242467) for large-area solar cell fabrication and characterization. J. E. was supported by the Princeton Alliance for Collaborative Research and Innovation. Q. Z. was supported by NSF-PREM grant #DMR-1826886. The steady-state PL and TRPL equipment used in this work was supported by the National Science Foundation Research Initiation Award: Novel Perovskite Solar Cells Based on Interface Manipulation (Award#1900047). Q. D. G. M., X. G. thank NSF grant OIA-1757220 for providing financial support for the 2D GIWAXS measurements.

Data Availability Statement: The authors declare that the data presented in this article are available from the authors upon reasonable request.

References

1. Jeong, J.; Kim, M.; Seo, J.; Lu, H.; Ahlawat, P.; Mishra, A.; Yang, Y.; Hope, M. A.; Eickemeyer, F. T.; Kim, M.; Yoon, Y. J.; Choi, I. W.; Darwich, B. P.; Choi, S. J.; Jo, Y.; Lee, J. H.; Walker, B.; Zakeeruddin, S. M.; Emsley, L.; Rothlisberger, U.; Hagfeldt, A.; Kim, D. S.;

Gratzel, M.; Kim, J. Y. Pseudo-Halide Anion Engineering for alpha-$FAPbI_3$ Perovskite Solar Cells. *Nature* **2021,** *592*, 381.

2. Min, H.; Lee, D. Y.; Kim, J.; Kim, G.; Lee, K. S.; Kim, J.; Paik, M. J.; Kim, Y. K.; Kim, K. S.; Kim, M. G.; Shin, T. J.; Il Seok, S. Perovskite Solar Cells with Atomically Coherent Interlayers on SnO_2 Electrodes. *Nature* **2021,** *598*, 444.

3. Park, J.; Kim, J.; Yun, H. S.; Paik, M. J.; Noh, E.; Mun, H. J.; Kim, M. G.; Shin, T. J.; Seok, S. I. Controlled Growth of Perovskite Layers with Volatile Alkylammonium Chlorides. *Nature* **2023,** *616*, 724.

4. Yun, H.-S.; Kwon, H. W.; Paik, M. J.; Hong, S.; Kim, J.; Noh, E.; Park, J.; Lee, Y.; Il Seok, S. Ethanol-Based Green-Solution Processing of α-Formamidinium Lead Triiodide Perovskite Layers. *Nat. Energy* **2022,** *7*, 828.

5. Kim, G.; Min, H.; Lee, K. S.; Lee, D. Y.; Yoon, S. M.; Seok, S. I. Impact of Strain Relaxation on Performance of α-Formamidinium Lead Iodide Perovskite Solar Cells. *Science* **2020,** *370*, pp.108.

6. Duan, L.; Zhang, H.; Liu, M.; Grätzel, M.; Luo, J. Phase-Pure γ-CsPbI3 for Efficient Inorganic Perovskite Solar Cells. *ACS Energy Lett.* **2022,** *7*, 2911.

7. Wang, J.; Che, Y.; Duan, Y.; Liu, Z.; Yang, S.; Xu, D.; Fang, Z.; Lei, X.; Li, Y.; Liu, S. F. 21.15%-Efficiency and Stable gamma -$CsPbI_3$ Perovskite Solar Cells Enabled by an Acyloin Ligand. *Adv. Mater.* **2023,** *35*, e2210223.

8. Che, Y.; Liu, Z.; Duan, Y.; Wang, J.; Yang, S.; Xu, D.; Xiang, W.; Wang, T.; Yuan, N.; Ding, J.; Liu, S. F. Hydrazide Derivatives for Defect Passivation in Pure $CsPbI_3$ Perovskite Solar Cells. *Angew Chem. Int. Ed. Engl.* **2022,** *61*, e202205012.

9. Yoon, S. M.; Min, H.; Kim, J. B.; Kim, G.; Lee, K. S.; Seok, S. I. Surface Engineering of Ambient-Air-Processed Cesium Lead Triiodide Layers for Efficient Solar Cells. *Joule* **2021,** *5*, 183.

10. Cui, Y.; Shi, J.; Meng, F.; Yu, B.; Tan, S.; He, S.; Tan, C.; Li, Y.; Wu, H.; Luo, Y.; Li, D.; Meng, Q. A Versatile Molten-Salt Induction Strategy to Achieve Efficient $CsPbI_3$ Perovskite Solar Cells with a High Open-Circuit Voltage >1.2 V. *Adv. Mater.* **2022,** *34*, e2205028.

11. Zhang, H.; Xiang, W.; Zuo, X.; Gu, X.; Zhang, S.; Du, Y.; Wang, Z.; Liu, Y.; Wu, H.; Wang, P.; Cui, Q.; Su, H.; Tian, Q.; Liu, S. F. Fluorine-Containing Passivation Layer via Surface Chelation for Inorganic Perovskite Solar Cells. *Angew Chem. Int. Ed. Engl.* **2023,** *62*, e202216634.

12. Wu, C.; Wang, K.; Li, J.; Liang, Z.; Li, J.; Li, W.; Zhao, L.; Chi, B.; Wang, S. Volatile Solution: The Way Toward Scalable Fabrication of Perovskite Solar Cells? *Matter* **2021,** *4*, 775.

13. Lee, S. H.; Hong, S.; Kim, H. J. Selection of a Suitable Solvent Additive for 2-Methoxyethanol-Based Antisolvent-Free Perovskite Film Fabrication. *ACS Appl. Mater. Interfaces* **2022,** *14*, 39132.

14. Deng, Y.; Van Brackle, C. H.; Dai, X.; Zhao, J.; Chen, B.; Huang, J. Tailoring Solvent Coordination for High-Speed, Room-Temperature Blading of Perovskite Photovoltaic Films. *Sci. Adv.* **2019,** *5*, p.eaax7537.

15. Yoo, J. W.; Jang, J.; Kim, U.; Lee, Y.; Ji, S.-G.; Noh, E.; Hong, S.; Choi, M.; Seok, S. I. Efficient Perovskite Solar Mini-Modules Fabricated Via Bar-Coating Using 2-Methoxyethanol-Based Formamidinium Lead Tri-Iodide Precursor Solution. *Joule* **2021,** *5*, 2420.

16. Abate, S. Y.; Yang, Z.; Jha, S.; Ma, G.; Ouyang, Z.; Zhang, H.; Muhammad, S.; Pradhan, N.; Gu, X.; Patton, D.; Wang, K.; Li, D.; Cai, J.; Dai, Q. Room Temperature Slot-Die Coated

Perovskite Layer Modified With Sulfonyl-γ-AApeptide for High Performance Perovskite Solar Devices. *Chem. Eng. J.* **2023,** *457*, 141199.

17. Li, J.; Dagar, J.; Shargaieva, O.; Flatken, M. A.; Köbler, H.; Fenske, M.; Schultz, C.; Stegemann, B.; Just, J.; Többens, D. M.; Abate, A.; Munir, R.; Unger, E. 20.8% Slot-Die Coated $MAPbI_3$ Perovskite Solar Cells by Optimal DMSO-Content and Age of 2-ME Based Precursor Inks. *Adv. Energy Mater.* **2021,** *11*.

18. Kwon, N.; Lee, J.; Ko, M. J.; Kim, Y. Y.; Seo, J. Recent Progress of Eco-Friendly Manufacturing Process of Efficient Perovskite Solar Cells. *Nano Converg.* **2023,** *10*, pp.1.

19. Küffner, J.; Hanisch, J.; Wahl, T.; Zillner, J.; Ahlswede, E.; Powalla, M. One-Step Blade Coating of Inverted Double-Cation Perovskite Solar Cells from a Green Precursor Solvent. *ACS Appl. Energy Mater.* **2021,** *4*, 11700.

20. Wang, K.; Wu, C.; Hou, Y.; Yang, D.; Ye, T.; Yoon, J.; Sanghadasa, M.; Priya, S. Isothermally Crystallized Perovskites at Room-Temperature. *Energy Environ. Sci.* **2020,** *13*, 3412.

21. Lee, D.-K.; Jeong, D.-N.; Ahn, T. K.; Park, N.-G. Precursor Engineering for a Large-Area Perovskite Solar Cell with >19% Efficiency. *ACS Energy Lett.* **2019,** *4*, 2393.

22. Sun, B.; Wang, W.; Lu, H.; Chao, L.; Gu, H.; Tao, L.; Hu, J.; Li, B.; Zong, X.; Shi, W.; Ran, X.; Zhang, H.; Xia, Y.; Li, P.; Chen, Y. Tuning the Interactions of Methylammonium Acetate with Acetonitrile to Create Efficient Perovskite Solar Cells. *J. Phys. Chem. C* **2021,** *125*, 6555.

23. Cassella, E. J.; Spooner, E. L. K.; Smith, J. A.; Thornber, T.; O'Kane, M. E.; Oliver, R. D. J.; Catley, T. E.; Choudhary, S.; Wood, C. J.; Hammond, D. B.; Snaith, H. J.; Lidzey, D. G. Binary Solvent System Used to Fabricate Fully Annealing-Free Perovskite Solar Cells. *Adv. Energy Mater.* **2023,** *13*, 2203468.

24. Belay Adugna, G.; Yimer Abate, S.; Tao, Y.-T. High-Efficiency and Scalable Solution-Sheared Perovskite Solar Cells Using Green Solvents. *Chem. Eng. J.* **2022,** *437*.

25. Jeong, D.-N.; Lee, D.-K.; Seo, S.; Lim, S. Y.; Zhang, Y.; Shin, H.; Cheong, H.; Park, N.-G. Perovskite Cluster-Containing Solution for Scalable D-Bar Coating toward High-Throughput Perovskite Solar Cells. *ACS Energy Lett.* **2019,** *4*, 1189.

26. Abate, S. Y.; Yang, Z.; Jha, S.; Emodogo, J.; Ma, G.; Ouyang, Z.; Muhammad, S.; Pradhan, N.; Gu, X.; Patton, D.; Li, D.; Cai, J.; Dai, Q. Promoting Large-Area Slot-Die-Coated Perovskite Solar Cell Performance and Reproducibility by Acid-Based Sulfono-gamma-AApeptide. *ACS Appl. Mater. Interfaces* **2023,** *15*, 25495.

27. O'Kane, M. E.; Smith, J. A.; Kilbride, R. C.; Spooner, E. L. K.; Duif, C. P.; Catley, T. E.; Washington, A. L.; King, S. M.; Parnell, S. R.; Parnell, A. J. Exploring Nanoscale Structure in Perovskite Precursor Solutions Using Neutron and Light Scattering. *Chem. Mater.* **2022,** *34*, 7232.

28. Flatken, M. A.; Hoell, A.; Wendt, R.; Härk, E.; Dallmann, A.; Prause, A.; Pascual, J.; Unger, E.; Abate, A. Small-Angle Scattering to Reveal the Colloidal Nature of Halide Perovskite Precursor Solutions. *J. Mater. Chem. A* **2021,** *9*, 13477.

29. Boonmongkolras, P.; Kim, D.; Alhabshi, E. M.; Gereige, I.; Shin, B. Understanding Effects of Precursor Solution Aging in Triple Cation Lead Perovskite. *RSC Adv.* **2018,** *8*, 21551.

30. Kim, J.; Park, B. W.; Baek, J.; Yun, J. S.; Kwon, H. W.; Seidel, J.; Min, H.; Coelho, S.; Lim, S.; Huang, S.; Gaus, K.; Green, M. A.; Shin, T. J.; Ho-Baillie, A. W. Y.; Kim, M. G.; Seok, S. I. Unveiling the Relationship between the Perovskite Precursor Solution and the Resulting Device Performance. *J. Am. Chem. Soc.* **2020,** *142*, 6251.

31. Singh, R. K.; Kumar, R.; Jain, N.; Dash, S. R.; Singh, J.; Srivastava, A. Investigation of Optical and Dielectric Properties of $CsPbI_3$ Inorganic Lead Iodide Perovskite Thin Film. *J. Taiwan Inst. Chem. Eng.* **2019,** *96*, 538.

32. Abate, S. Y.; Jha, S.; Ma, G.; Nash, J.; Pradhan, N.; Gu, X.; Patton, D.; Dai, Q. Surface Capping Layer Prepared from the Bulky Tetradodecylammonium Bromide as an Efficient Perovskite Passivation Layer for High-Performance Perovskite Solar Cells. *ACS Appl. Mater. Interfaces* **2022,** *14*, 56900.

33. Christians, J. A.; Manser, J. S.; Kamat, P. V. Best Practices in Perovskite Solar Cell Efficiency Measurements. Avoiding the Error of Making Bad Cells Look Good. *J. Phys. Chem. Lett.* **2015,** *6*, 852.

34. Abate, S. Y.; Wu, W. T.; Pola, S.; Tao, Y. T. Compact TiO_2 Films with Sandwiched Ag Nanoparticles as Electron-Collecting Layer in Planar Type Perovskite Solar Cells: Improvement in Efficiency and Stability. *RSC Adv.* **2018,** *8*, 7847.

35. Abate, S. Y.; Zhang, Q.; Qi, Y.; Nash, J.; Gollinger, K.; Zhu, X.; Han, F.; Pradhan, N.; Dai, Q. Universal Surface Passivation of Organic-Inorganic Halide Perovskite Films by Tetraoctylammonium Chloride for High-Performance and Stable Perovskite Solar Cells. *ACS Appl. Mater. Interfaces* **2022,** *14*, 28044.

36. Adugna, G. B.; Abate, S. Y.; Wu, W. T.; Tao, Y. T. Toward Large-Area and Fully Solution-Sheared Perovskite Solar Cells. *ACS Appl. Mater. Interfaces* **2021,** *13*, 25926.

37. Abate, S. Y.; Huang, D.-C.; Tao, Y.-T. Surface Modification of TiO_2 Layer With Phosphonic Acid Monolayer in Perovskite Solar Cells: Effect of Chain Length and Terminal Functional Group. *Org. Electron.* **2020,** *78*, 105583.

TOC

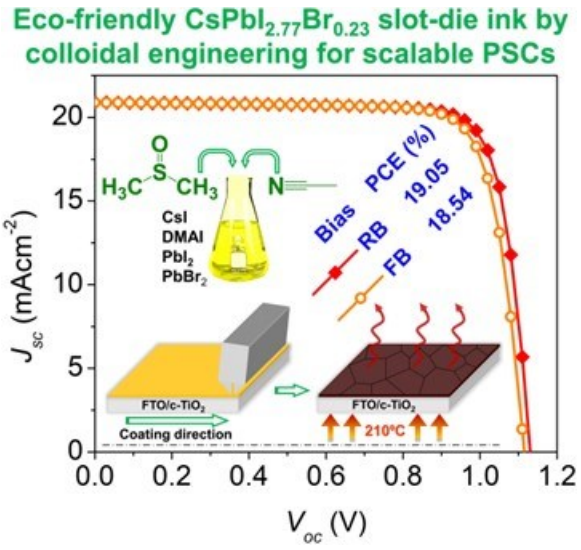

We developed $CsPbI_{2.77}I_{0.23}$ slot-die inks via the colloidal engineering of scalable large-area perovskite solar cells. Eco-friendly solvents such as dimethyl sulfoxide (DMSO), acetonitrile (ACN), and 2-methoxyethanol (2-ME) were used. Film growth was controlled by varying the solvent ratio. The cells based on films prepared by slot-die coating exhibited an efficiency of 19.05 %.